AIP Applied Physics Letters

Microfluidic emulsification through a monolithic integrated glass micronozzle suspended inside a flow-focusing geometry

Yifan Liu and Levent Yobas

Citation: Applied Physics Letters **106**, 174101 (2015); doi: 10.1063/1.4919444
View online: http://dx.doi.org/10.1063/1.4919444
View Table of Contents: http://scitation.aip.org/content/aip/journal/apl/106/17?ver=pdfcov
Published by the AIP Publishing

Articles you may be interested in

Dynamics of step-emulsification: From a single to a collection of emulsion droplet generators
Phys. Fluids **26**, 082109 (2014); 10.1063/1.4892949

Corrugated interfaces in multiphase core-annular flow
Phys. Fluids **22**, 082002 (2010); 10.1063/1.3480561

Wetting gradient induced separation of emulsions: A combined experimental and lattice Boltzmann computer simulation study
Phys. Fluids **20**, 072104 (2008); 10.1063/1.2963958

Controlled production of emulsion drops using an electric field in a flow-focusing microfluidic device
Appl. Phys. Lett. **91**, 133106 (2007); 10.1063/1.2790785

Generation of monodisperse gel emulsions in a microfluidic device
Appl. Phys. Lett. **88**, 024106 (2006); 10.1063/1.2164393

This article is copyrighted as indicated in the article. Reuse of AIP content is subject to the terms at: http://scitation.aip.org/termsconditions. Downloaded to IP: 202.40.139.130 On: Mon, 29 Jun 2015 04:40:00

Microfluidic emulsification through a monolithic integrated glass micronozzle suspended inside a flow-focusing geometry

Yifan Liu and Levent Yobas[a)]
Department of Electronic and Computer Engineering, The Hong Kong University of Science and Technology, Hong Kong, People's Republic of China

(Received 28 January 2015; accepted 19 April 2015; published online 28 April 2015)

Microfluidic devices have shown remarkable success in generating emulsions with precise control over their size. Yet, highly sensitive nature of generation mechanism to surface wettability requires such devices to be built out of specific materials showing homogenous wettability that favors the continuous phase rather than the dispersed phase. Moreover, the need to switch the continuous phase and the dispersed phase requires switching the device wettability by applying a suitable surface treatment. Here, we demonstrate a microfluidic device that can generate water-in-oil and oil-in-water emulsions without the necessity of surface treatment. The device features a suspended glass micronozzle integrated inside a flow-focusing geometry formed by silicon and poly(dimethylsiloxane) channels where drops of the dispersed phase can be sheared off at the micronozzle tip without touching channel walls in a coflow of the continuous phase. The micronozzle structure is a partially released segment of a self-enclosed capillary entirely built in phosphosilicate glass and with a cylindrical lumen ~1.5 μm in diameter. Owing to high fluidic resistance of such fine capillary, emulsion generation in the device takes place in a dripping process and no noticeable jet formation of the dispersed phase has been observed throughout the tested flow rates. The effect of the flow rates on the diameter of the emulsions and their rate of generation has been experimentally investigated and found to show a similar trend to that of a simple physical model based on the critical Capillary number. © *2015 AIP Publishing LLC*. [http://dx.doi.org/10.1063/1.4919444]

Droplet microfluidics has attracted tremendous attention for its utmost value in chemical and biological research.[1] Droplets or emulsions provide extremely small encapsulated compartments, which enable rapid mixing of fluids[2] and controlled reaction of chemical reagents.[3] Reproducible generation of emulsions and their highly controllable manipulation have made droplet microfluidics an ideal platform for a diverse set of applications including digital microanalysis,[4] therapeutic agent delivery,[5] biomolecule synthesis,[6] and functional material fabrication.[7]

A wealth of microfluidic strategies has been demonstrated to generate controllable and monodisperse emulsions. Notably, Thorsen *et al*.[8] developed a T-junction, in which a stream of oil crosses a water stream and shears off water droplets. Anna *et al*.[9] showed an integrated flow-focusing geometry and produced both monodisperse and polydisperse emulsions. A 3D flow-focusing geometry was demonstrated featuring a high-performance spontaneous generation of monodisperse droplets.[10] Comprehensive reviews were also given on the topic.[11]

Generating both water-in-oil and oil-in-water droplets on the same device is essential for important applications such as those involving multiple emulsions.[12] However, this usually requires extra effort on precisely and site-specifically modifying the surface wettability of microchannel walls,[13] which is cumbersome and not favored in terms of laborsaving. Chu *et al*.[14] demonstrated a clever microfluidic design for droplet generation that relaxes the wetting constraints. The device is an assembly of glass capillaries; a tapered glass capillary is inserted in the center of a larger capillary, thereby forming a coaxial hydrodynamic flow-focusing geometry. In this configuration, the generated droplets travel only in the center stream of the continuous phase without touching the capillary wall. Nevertheless, concerns remain in the robustness and manufacturability of the system in order to facilitate its widespread use. Thus, a monolithic integration of similar coaxial flow geometry is highly desired. Implementing such configuration on chip is challenging in terms of both the fabrication of a suspended capillary/nozzle and its microfluidic integration. Although Kim *et al*.[15] fabricated protruding silica micronozzles based on thermal oxidation of bonded silicon wafers, the process does not render itself for integrating such micronozzles into a microfluidic channel suitable for droplet applications.

Glass thermal reflow has been recently introduced by our group as a route to fabricate round capillaries based on the shape transformation of voids being trapped inside silicon trenches partially filled with a glass layer.[16] Leveraging this process, we demonstrate here an integrated microfluidic device for monodisperse generation of both water-in-oil and oil-in-water droplets without the requirement of patterning surface wettability. Fig. 1(a) schematically describes the device structure with the cover plate partially drawn. In the device, a single suspended glass micronozzle is integrated within a flow-focusing geometry on silicon and supplied with a fluid (discrete phase) through a channel at the opposing end. The emulsions are generated at the micronozzle tip in the coflowing stream of a second immiscible fluid (continuous phase) introduced through the side channels. In such a

[a)]Author to whom correspondence should be addressed. Electronic mail: eelyobas@ust.hk

 © 2015 AIP Publishing LLC

This article is copyrighted as indicated in the article. Reuse of AIP content is subject to the terms at: http://scitation.aip.org/termsconditions. Downloaded to IP: 202.40.139.130 On: Mon, 29 Jun 2015 04:40:00

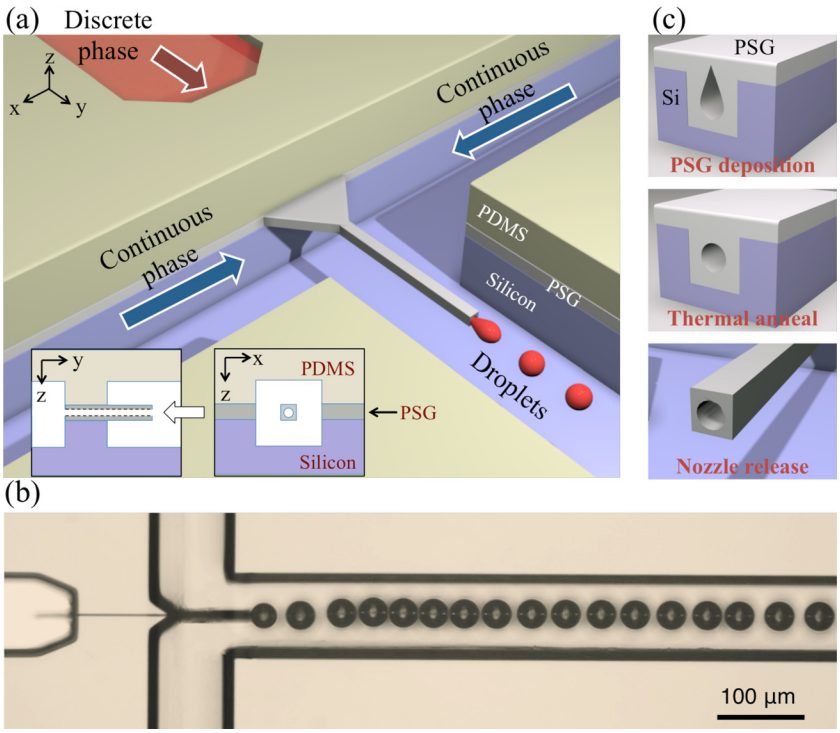

FIG. 1. (a) 3D rendering of the microfluidic device featuring a single suspended micronozzle integrated inside a flow-focusing geometry between a silicon substrate and a PDMS cover plate (shown in part for clarity). The micronozzle is entirely defined in a PSG layer. The insets are the cross-sectional illustrations. (b) Monodisperse drops of discrete phase (water) within a coflow of continuous phase (mineral oil) depicted forming at the tip of a 100-μm-long micronozzle. (c) Major fabrication steps.

configuration, the droplets travel downstream following the center stream without touching channel walls as a result of hydrodynamic focusing of the coaxial flow, Fig. 1(b), which enables the generation of both water-in-oil and oil-in-water emulsions being free of surface wettability. Thus, the device employs a similar mechanism to that of the manually assembled glass capillaries[14] and yet introduces an integrated approach that is more robust and mass producible.

The device fabrication involved the formation of a self-enclosed round capillary and its subsequent release to define the suspended micronozzle and flow-focusing channels, Fig. 1(c). Briefly, a layer of phosphosilicate glass (PSG), 5 μm thick, was deposited through low-pressure chemical vapor deposition (LPCVD) on silicon featuring a trench, 3 μm wide and deep, created by deep reactive ion etch (DRIE). The nonconformal step coverage profile of this layer left an elongated void trapped within the trench, which was subsequently transformed into a cylindrical tube through glass reflow under surface tension during a thermal anneal step performed in N_2 ambient (1000 °C for 1 h). The microfluidic integration of the capillary into the flow-focusing geometry as a suspended micronozzle was realized through standard photolithography and subsequent dry etching steps; the PSG layer was removed first by advanced oxide etch (AOE) through the resist mask and then the exposed silicon was etched by DRIE to a depth of 40 μm. Not only did these steps form the channels but also they cut open both ends of the capillary and outlined the capillary segment that would be released into a suspended micronozzle. The subsequent release step took place in SF_6 plasma and left the channels with an overall depth of 50 μm.

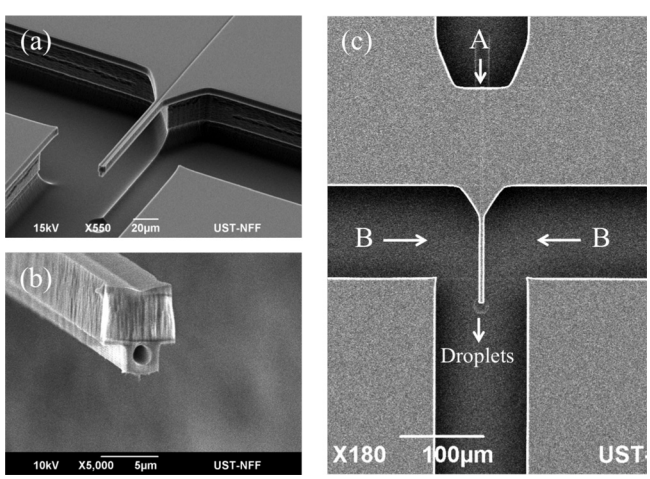

FIG. 2. SEM: (a) isometric view of the flow-focusing geometry with the suspended micronozzle, (b) close-up view of the micronozzle tip revealing the circular opening, and (c) planar view of the microfluidic design with the arrows denoting the flow directions A for discrete phase and B for continuous phase.

Fig. 2 depicts scanning electron micrographs (SEMs) of the flow-focusing geometry taken from a representative device in various perspectives. The 100-μm long suspended micronozzle features a round opening ~1.5 μm in diameter, Fig. 2(b). Before the experiments, a polydimethylsiloxane (PDMS) cap was secured on the chip through oxygen plasma activation to form the inlet/outlet ports. In order to situate the micronozzle in the center of the fluidic channel, the PDMS cap was pre-structured with the same flow-focusing layout (50 μm in height) through soft lithography and carefully aligned to the chip with the aid of a microscope. To generate droplets, the dispersed and continuous phases were delivered into the respective channels using a syringe pump (Harvard Apparatus) for each liquid in the directions denoted in Fig. 2(c). Distilled water (viscosity 0.9 mPa s at 24 °C) was used with either hexadecane (viscosity 3.34 mPa s, density 773 kg/m^3, Sigma Aldrich) as the dispersed phase or pure silicone fluid (viscosity 10 cSt, density 935 kg/m^3, Clearco) as the continuous phase. The interfacial tension between the immiscible phases was 47 and 24 mN/m,

This article is copyrighted as indicated in the article. Reuse of AIP content is subject to the terms at: http://scitation.aip.org/termsconditions. Downloaded to IP: 202.40.139.130 On: Mon, 29 Jun 2015 04:40:00

respectively.[17] No surfactant or plasma treatment was used. We measured the rate of droplet formation f by counting the generated droplets within a specified time interval, whereas diameter of the droplets D was acquired by direct measurements on the still images recorded. The images were captured under a microscope (Nikon) using a high-speed camera (Phantom, Vision Research).

The generation of water-in-oil droplets was performed in a unit featuring a 20-μm long micronozzle. Fig. 3(a) presents the frame-by-frame formation of individual monodispersed water droplets at a fixed outer flow rate $Q_{out} = 0.8$ ml/h and a fixed inner flow rate Q_{in} which is an insignificant fraction of the set value of the respective syringe pump Q_{set}, at 0.2 ml/h, i.e., $Q_{in} = \alpha Q_{set}$, where α is typically below 1% depending on the hydraulic resistance of the micronozzle. For this condition, the measured droplet diameter and generation rate refer to $\sim$42 μm and $\sim$17.8 Hz, respectively. The droplet formation in our device can be described by the dripping mechanism.[18] In the dripping regime, a droplet growing in a coflowing outer fluid experiences two competing forces: a viscous drag force, F_{drag}, pulling the droplet downstream and an interfacial tension force, F_γ, holding it on the micronozzle tip. The relative importance of the two opposing forces are given by the Capillary number, $\mathrm{Ca} = F_{drag}/F_\gamma$. The interfacial tension force dominates initially, but then the increasing drag force becomes significant as the droplet grows and leads to its separation from the micronozzle tip. The dripping dynamics can be accurately modeled by a simple analytic expression that features a single fitting parameter: the critical Capillary number, Ca_{crit}.[19] This model has been recently applied to emulsions produced in the manually assembled glass capillaries and shown to predict the droplet diameter, D, based on a single universal value that leads to the droplet rupture, $\mathrm{Ca}_{crit} \sim 0.1$.[19] By adopting the model here, the droplet rupture is similarly assumed to occur at

$$\mathrm{Ca} \geq \mathrm{Ca}_{crit}. \tag{1}$$

The interfacial tension force holding the emerging droplet on the micronozzle tip is given by

$$F_\gamma = \pi \gamma d_{tip}, \tag{2}$$

where γ is the interfacial tension between the two immiscible fluids and d_{tip} is the micronozzle tip size. Note that d_{tip} is the characteristic tip size and assigned here as 6 μm based on SEM measurements, Fig. 2(b). The viscous drag force acting on the droplet protruding from the tip can be expressed by a modified Stokes formula after taking into account the shielding effect of the micronozzle tip

$$F_{drag} = 3\pi\eta_{out}(D - d_{tip})\,(u_{out} - u_{in}), \tag{3}$$

where η_{out} is the viscosity of the outer fluid, whereas u_{out} and u_{in} are the average velocities of the outer and inner fluids, respectively. These velocities can be estimated from their respective volumetric flow rates, Q_{out} and Q_{in}, and their associated cross-sectional areas: $u_{out} = 4Q_{out}/(4A - \pi D^2)$ and $u_{in} = 4Q_{in}/\pi D^2$, where A is the cross-sectional area of the collection channel that measures 100 μm wide and deep. Due to the large hydraulic resistance imposed by the micronozzle, Q_{in} remains far below the set value of the respective pump, Q_{set}, and thus Q_{out}. Accordingly, the velocity of the inner fluid within the protruding droplet is negligible compared to that of the outer fluid ($u_{out} \gg u_{in}$). The above equations lead to the following quadratic relation with only one practical solution

$$k\hat{D}^2 + \mathrm{Ca}_{norm}\hat{D} - (1 + \mathrm{Ca}_{norm}) = 0, \tag{4}$$

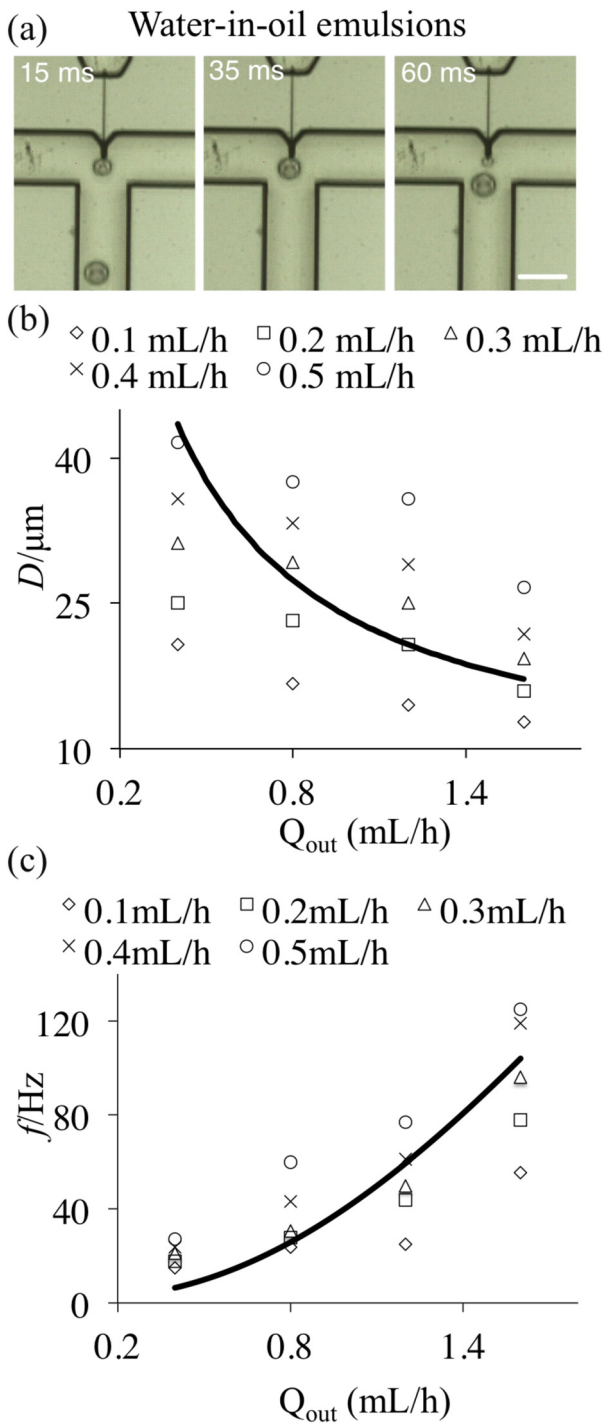

FIG. 3. Water-in-oil emulsions. (a) Time-lapse images showing a single water droplet forming at the micronozzle tip in a coflow of oil. (b) Droplet diameter D and (c) droplet generation rate f plotted as a function of oil flow rate Q_{out} for distinct set values of the water pump Q_{set} (legend). The solid curves are the corresponding fittings obtained with $\mathrm{Ca}_{crit} = 0.1$ and $Q_{in} = 1$ μl/h by Eqs. (5) and (6). Scale: 100 μm.

This article is copyrighted as indicated in the article. Reuse of AIP content is subject to the terms at: http://scitation.aip.org/termsconditions. Downloaded to IP: 202.40.139.130 On: Mon, 29 Jun 2015 04:40:00

where k denotes the ratio of the cross-sectional area of the micronozzle tip to that of the channel, d_{tip}^2/A, $\hat{D}$ refers to the diameter of the protruding droplet with respect to the size of the micronozzle tip, D/d_{tip}, and $\mathrm{Ca}_{\mathrm{norm}}$ is defined here as the ratio of $\mathrm{Ca}_{\mathrm{tip}}/\mathrm{Ca}_{\mathrm{crit}}$, with $\mathrm{Ca}_{\mathrm{tip}}$ representing the relative importance of the viscous drag force at the micronozzle tip against the interfacial tension force for a newly forming droplet, i.e., $F_{\mathrm{drag}}^{\mathrm{tip}}/F_{\gamma}$, where $F_{\mathrm{drag}}^{\mathrm{tip}} \sim 3\pi\eta_{\mathrm{out}} d_{\mathrm{tip}} Q_{\mathrm{out}}/A$.

Thus, Eq. (4) can be solved to obtain the scaled droplet diameter

$$\hat{D} = \frac{\mathrm{Ca}_{\mathrm{norm}}}{2k}\left(-1 + \sqrt{1+\Delta}\right), \tag{5}$$

where $\Delta = 4k(1 + \mathrm{Ca}_{\mathrm{norm}})/\mathrm{Ca}_{\mathrm{norm}}^2$.

Equation (5) predicts that, for a given inner/outer fluid and micronozzle/channel dimensions, the diameter of the detaching droplet decreases as Q_{out} increases. Considering the conservation of mass, the generation rate of droplets can be stated as $f \sim 6Q_{\mathrm{in}}/\pi D^3$ or alternatively in u_{in} and $\hat{D}$ as

$$f \sim \frac{3}{2}\frac{u_{\mathrm{in}}}{d_{\mathrm{tip}}}\hat{D}^{-1}. \tag{6}$$

In Figs. 3(b) and 3(c), the formation of water droplets are compared at increasing oil flow rates for distinct set values of the water pump Q_{set} (legend). The trends observed here are in agreement with the predictions of the model given by Eqs. (5) and (6). However, the model predictions also suggest that the volumetric flow rate through the micronozzle, Q_{in}, remains limited to a small fraction of the pump set value Q_{set} (α below $\sim$1%). This is reasonable because even for such a low flow rate, $Q_{\mathrm{in}} \sim 1\ \mu$l/h, pressure drop across the micronozzle amounts to nearly 3.25 bar which is estimated based on the parabolic flow profile through the tube diameter 0.75 μm and length 140 μm (inclusive of the suspended 20-μm-long segment). Meanwhile, the majority of the flow is compensated by the hydraulic capacitance of the compliant tubing interface and PDMS cover. Although the droplet diameter according to Eq. (5) is expected to remain unchanged irrespective of Q_{in} (thus Q_{set}), one can notice size variations across droplets obtained with distinct levels of Q_{set}, at a fixed Q_{out}, Fig. 3(b). Such discrepancy is not observed in the case of oil-in-water droplets generated in a device featuring a 100-μm-long micronozzle, Fig. 4(b), suggesting that the discrepancy might stem from the position of the micronozzle tip within the flow-focusing geometry where droplets break free. The oil droplets were sheared off from the protruding micronozzle tip inside the collection channel, Fig. 4(a), whereas the water droplets were pinched off right at the junction without a fully developed coflowing stream of the oil phase. This might have entailed forces and flow types other than simple shear and hence introduced the observed size dependence of droplets on the dispersed phase flow.

Unlike the water-in-oil droplets, the oil-in-water droplets were generated at higher continuous flow rates; at relatively low water flow rates, the oil droplet interestingly sticks on the glass micronozzle tip that ought to be hydrophilic. This is probably due to the high surface roughness of the sidewall glass left by dry etching, Fig. 2(b), or the polymer film coatings deposited on the micronozzle surface during etching. Fig. 4(a) presents time-lapse micrographs showing the formation of an oil-in-water droplet at a fixed outer flow rate $Q_{\mathrm{out}} = 10$ ml/h and fixed inner flow rate corresponding to $Q_{\mathrm{set}} = 0.2$ ml/h. The device used here features a relatively long micronozzle extending 100-μm long. The generation rate and droplet diameter were measured as $\sim$7.0 Hz and $\sim$38 μm, respectively. Fig. 4(b) shows the diameters of generated oil droplets plotted as a function of water (outer) flow rates for distinct set values of the oil pump, Q_{set} (legend). As seen, the droplet diameter is fairly

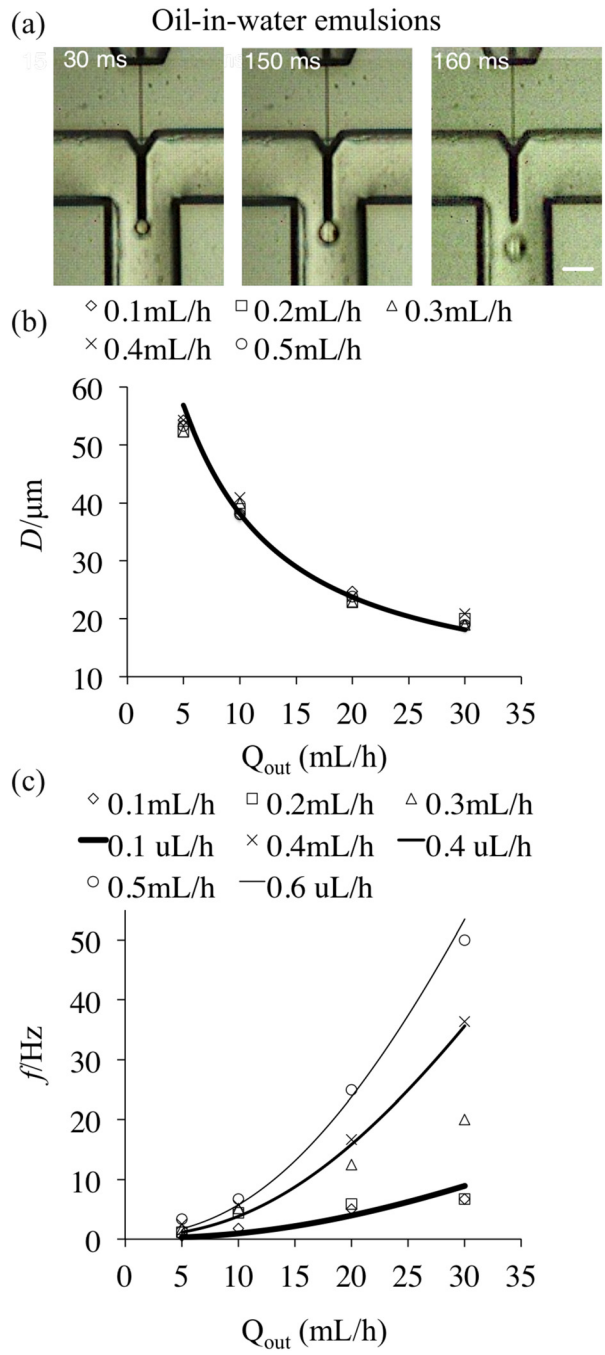

FIG. 4. Oil-in-water emulsions. (a) Time-lapse images showing a single oil droplet forming at the micronozzle tip in a coflow of water. (b) Droplet diameter D and (c) droplet generation rate f plotted as a function of water flow rate Q_{out} for distinct set values of the oil pump Q_{set} (legend). The solid curves are the respective fittings obtained with $\mathrm{Ca}_{\mathrm{crit}} = 0.1$ and for distinct values of Q_{in} (legend) by Eqs. (5) and (6). Scale: 50 μm.

This article is copyrighted as indicated in the article. Reuse of AIP content is subject to the terms at: http://scitation.aip.org/termsconditions. Downloaded to IP: 202.40.139.130 On: Mon, 29 Jun 2015 04:40:00

independent of the oil flow rate, which is in accordance with the model and unlike the case of the water-in-oil droplets formed in the device with the relatively short micronozzle (20 μm). The droplet diameter decreases inversely with the continuous (water) flow rate, in strong agreement with Eq. (5). Meanwhile, the generation rate increases drastically with the increase of water flow rate, in agreement with Eq. (6) based on the assumption of $\alpha \sim 0.1\%$, as presented in Fig. 4(c).

It is worth noting that liquid jetting was not observed in our device for both water-in-oil and oil-in-water emulsions. In a previous work by Utada *et al.*,[18] the dripping to jetting transition was studied in coflowing liquid streams based on a coaxial capillary assembly and found to occur in two distinct classes. The first class of transition is driven by the flow rate of the outer continuous phase and occurs spontaneously when the capillary number of the outer continuous phase becomes increasingly large, i.e., $\mathrm{Ca}_{\mathrm{out}} \geq O(1)$. This capillary number, $\mathrm{Ca}_{\mathrm{out}} = \eta_{\mathrm{out}} u_{\mathrm{out}}/\gamma$, corresponds to $\mathrm{Ca}_{\mathrm{tip}}$ in our model and hardly exceeded 0.05 here. The second class of transition to jetting is driven by an excessive increase of the inner flow rate which occurs when the Weber number of the inner dispersed phase, $\mathrm{W}_{\mathrm{in}} = \rho_{\mathrm{in}} d_{\mathrm{tip}} u_{\mathrm{in}}^2/\gamma$ with ρ_{in} is the dispersed phase density, gets equally large, i.e., $\mathrm{W}_{\mathrm{in}} \geq O(1)$. Yet, in our experiments, the inertia of the dispersed phase was extremely small and hence $\mathrm{W}_{\mathrm{in}} \ll 1$. While it is reasonable to expect the transition to jetting in our device with an increased outer flow rate to the extent that $\mathrm{Ca}_{\mathrm{out}} \geq O(1)$, it would be rather difficult to reach jetting through an increased inner flow rate, $\mathrm{W}_{\mathrm{in}} \geq O(1)$, due to the difficulty with setting an extremely large pressure drop across the micronozzle.

In conclusion, we have demonstrated a facile method of generating emulsions independent of the surface wettability using a monolithic device featuring a suspended glass micronozzle integrated into a microfluidic flow-focusing geometry. This device offers interesting possibilities for a set of applications such as multiple emulsions.

This research was supported by a grant from the Research Grant Council of Hong Kong (No. GRF621513).

[1]S. Y. Teh, R. Lin, L. H. Hung, and A. P. Lee, Lab Chip **8**, 198 (2008).
[2]J. D. Tice, H. Song, A. D. Lyon, and R. F. Ismagilov, Langmuir **19**, 9127 (2003).
[3]H. Song, D. L. Chen, and R. F. Ismagilov, Angew. Chem. Int. Ed. **45**, 7336 (2006).
[4]V. Srinivasan, V. K. Pamula, and R. B. Fair, Lab Chip **4**, 310 (2004).
[5]M. J. Lawrence and G. D. Rees, Adv. Drug Delivery Rev. **45**, 89 (2000).
[6]L. Mazutis, A. F. Araghi, O. J. Miller, J. C. Baret, L. Frenz, A. Janoshazi, V. Taly, B. J. Miller, J. B. Hutchison, D. Link, A. D. Griffiths, and M. Ryckelynck, Anal. Chem. **81**, 4813 (2009).
[7]I. Shestopalov, J. D. Tice, and R. F. Ismagilov, Lab Chip **4**, 316 (2004).
[8]T. Thorsen, R. W. Roberts, F. H. Arnold, and S. R. Quake, Phys. Rev. Lett. **86**, 4163 (2001).
[9]S. L. Anna, N. Bontoux, and H. A. Stone, Appl. Phys. Lett. **82**, 364 (2003).
[10]L. Yobas, S. Martens, W. L. Ong, and N. Ranganathan, Lab Chip **6**, 1073 (2006).
[11]R. Seemann, M. Brinkmann, T. Pfohl, and S. Herminghaus, Rep. Prog. Phys. **75**, 016601 (2012); C. N. Baroud, F. Gallaire, and R. Dangla, Lab Chip **10**, 2032 (2010); P. S. Dittrich and A. Manz, Nat. Rev. Drug Discovery **5**, 210 (2006).
[12]S. Okushima, T. Nisisako, T. Torii, and T. Higuchi, Langmuir **20**, 9905 (2004).
[13]A. R. Abate, J. Thiele, M. Weinhart, and D. A. Weitz, Lab Chip **10**, 1774 (2010).
[14]L. Y. Chu, A. S. Utada, R. K. Shah, J. W. Kim, and D. A. Weitz, Angew. Chem. Int. Ed. **46**, 8970 (2007).
[15]W. Kim, M. Q. Guo, P. D. Yang, and D. J. Wang, Anal. Chem. **79**, 3703 (2007).
[16]Y. F. Liu and L. Yobas, Biomicrofluidics **6**, 046502 (2012).
[17]S. van der Graaf, C. G. P. H. Schroen, R. G. M. van der Sman, and R. M. Boom, J. Colloid Interface Sci. **277**, 456 (2004).
[18]A. S. Utada, A. Fernandez-Nieves, H. A. Stone, and D. A. Weitz, Phys. Rev. Lett. **99**, 094502 (2007).
[19]R. M. Erb, D. Obrist, P. W. Chen, J. Studer, and A. R. Studart, Soft Matter **7**, 8757 (2011).

This article is copyrighted as indicated in the article. Reuse of AIP content is subject to the terms at: http://scitation.aip.org/termsconditions. Downloaded to IP: 202.40.139.130 On: Mon, 29 Jun 2015 04:40:00